Understanding the Capacity Decay of Si/NMC622 Li-ion Batteries Cycled in Superconcentrated Ionic Liquid Electrolytes: A New Perspective

Khryslyn Araño[a,b,c], Nicolas Gautier[a], Robert Kerr[b], Bernard Lestriez[a], Jean Le Bideau[a], Patrick C. Howlett[b], Dominique Guyomard[a], Maria Forsyth[b], and Nicolas Dupré[a,]*

[a]Université de Nantes, CNRS, Institut des Matériaux Jean Rouxel (IMN), F – 44000, Nantes, France

[b]Institute for Frontier Materials (IFM), Deakin University, 221 Burwood Highway, Burwood, Victoria 3125, Australia

[c]French Environment and Energy Management Agency 20, avenue du Grésillé- BP 90406 49004 Angers Cedex 01 France

*: corresponding author

KEYWORDS: lithium-ion batteries, silicon, anode, full cell, ionic liquid electrolytes, superconcentrated electrolytes

ABSTRACT: silicon-containing Li-ion batteries have been the focus of many energy storage research efforts because of the promise of high energy density. Depending on the system, silicon generally demonstrates stable performance in half cells, which is often attributed to the unlimited

lithium supply from the lithium (Li) metal counter electrode. Here, the electrochemical performance of silicon with a high voltage NMC622 cathode was investigated in superconcentrated phosphonium-based ionic liquid (IL) electrolytes. As a matter of fact, there is very limited work and understanding of the full cell cycling of silicon in.such a new class of electrolyte. The electrochemical behavior of silicon in the various IL electrolytes shows a gradual and steeper capacity decay, compared to what we previously reported in half cells. This behavior is linked to a different evolution of the silicon morphology upon cycling and the characterization of cycled electrodes points towards mechanical reasons, complete disconnection of part of the electrode, or internal mechanical stress, due to silicon and Li metal volume variation upon cycling, to explain the progressive capacity fading in full cell configuration. An extremely stable Solid Electrolyte Interphase (SEI) in the full Li-ion cells is seen from a combination of qualitative and quantitative information from TEM, XPS, EIS, and MAS NMR. Our findings provide a new perspective to full cell interpretation regarding capacity fading which is oftentimes linked almost exclusively to the loss of Li inventory but also more broadly, provide new insight on the impact of the evolution of silicon morphology on the electrochemical behavior.

1. INTRODUCTION

Lithium-ion batteries (LIBs) are generally considered to remain the battery technology of choice in the foreseeable future.[1] However, the rise of high-energy applications such as electric vehicles demands that LIBs meet their energy density requirements. As a negative electrode, silicon (Si) is a very attractive alternative to the state-of-the-art graphite [2] because of its very high theoretical capacity (3579 $mAh.g^{-1}$) [3] and low discharge potential. In addition, Si is naturally abundant and environmentally benign.[4,5] However, the widespread utilization of Si for batteries has been

impeded by the severe volumetric changes that accompany its lithiation and delithiation. This results in several other phenomena such as electrode disintegration and an unstable solid electrolyte interphase (SEI), which lead to the characteristic capacity fading observed in Si-containing LIBs.

The improved cycling behavior of Si in half cells is generally attributed to the large excess of cyclable lithium (Li) in the cell.[6] Indeed, the irreversible capacity loss in each cycle is compensated by the so-called "infinite lithium reservoir" of the Li metal negative electrode. Contrary to half cells, the amount of cyclable Li is limited by the Li content in the positive electrode material in a full cell format. This fundamental difference between the two configurations, in addition to the contribution of the positive electrode material, is projected to impart changes in the electrochemical behavior as well as in the resulting interfacial SEI properties of Si-based batteries. Moreover, the negative electrode/positive electrode capacity ratio is typically chosen to be slightly higher than 1, in order to avoid the lithium plating process during the Li-Si alloying reaction. Such a configuration can lead to an incomplete lithiation of the Si in the negative electrode and thus decreased mechanical constraints. It has been shown that weaker mechanical strains on Si, i.e. limited capacity cycling[7-10], can result in reduced electrode crack formation, pulverization of the Si particles and slowing down the rate of formation of the SEI.

Traditional ester-based carbonate electrolytes are unable to stabilize the Si anode interphase.[6,11,12] Several strategies have been explored to improve the stability of the Si/electrolyte interphase such as the use of artificial SEI[13,14], electrolyte additives[15-17], and mixed salt electrolyte[18]. In addition to these, there is also an increasing interest in the use of ionic liquids (IL), i.e., organic cation-anion mixture at liquid state, as an alternative to the classical carbonate electrolytes. ILs

have remarkable physicochemical properties such as non-flammability, low volatility, high thermal stability, and wide electrochemical window.[19] In particular, phosphonium-based ILs have been reported to exhibit electrochemical windows higher than 5 V.[20,21] Superconcentrated IL electrolytes of different chemistries show a superior behavior towards the stabilization of both Si and Li metal electrodes[22-24]. This class of ILs also displayed good compatibility with positive cathode materials. [23,25] In our previous work[12], we disclosed the promising behavior of Si in half cell in triethyl(methyl)phosphonium (P_{1222}) bis(fluorosulfonyl)imide (FSI) and *N*-methyl-*N*-propylpyrrolidinium (C_3mpyr) FSI with highly concentrated LiFSI salt (3.2 mol.kg^{-1}), where better capacity retention, i.e. ~80% after 100 cycles, was achieved using the IL with a phosphonium cation. The stability of Si in P_{1222}FSI with 3.2 m LiFSI, was linked to a more efficient and less resistive SEI composed mainly of LiFSI decomposition products such as LiF and other lithiated species such as trapped LiFSI salt,[22] that enabled good cycling.

However, to the best of our knowledge very little to no work has been performed towards the performance evaluation of Si anode in full cells with superconcentrated IL electrolytes[26] and none with the purpose to decipher the capacity fading mechanism upon cycling. Therefore, to fill this gap, we examine here the effect of phosphonium cation chemistry on the cycling behavior of Si paired with a high voltage $LiNi_{0.6}Mn_{0.2}Co_{0.2}O_2$ (NMC622) cathode and we demonstrate that the progressive capacity fading upon cycling is not due to a continuous Li ions trapping in the SEI. Moreover, an extremely stable SEI amount, from ^{19}F and ^{7}Li MAS-NMR quantification experiments, is found between the early stage of cycling and 100 cycles, showing that superconcentrated IL-based electrolytes are very promising to passivate efficiently the Si surface and to avoid an uncontrolled SEI growth. The evolutions of SEI and electrochemical behaviors in the case of half-cell and full-cell are then discussed.

2. EXPERIMENTAL SECTION

2.1 Electrode Preparation

Si nanoparticles (~150 nm diameter, S'tile)[27] were mixed with graphene nanoplatelets (GM15, length ~15 µm, width ~5-10 µm, S_{BET}: 74 m^2g^{-1}, XGSciences). The latter serves as a conductive additive. Mixing of these two components was performed using an agate mortar and pestle for about 2 minutes. A solution containing the binder, sodium carboxymethyl cellulose (Na-CMC, DS = 0.9, M_W = 700,000, Sigma Aldrich), and dispersant, polyacrylic co-maleic acid (average M_w 3,000, 50 wt. % in H_2O, Sigma Aldrich), in ultrapure water (< 0.05 µS cm^{-1}) plus a pH 3 buffer solution (citric acid and potassium hydroxide) was prepared by constant stirring for at least 3 hours to ensure the homogeneity of the solution. The Si-graphene mix and the prepared solution were then placed in a 12 ml silicon nitride jar, giving a total of 200 mg solids with a weight percent ratio of 71:7:11:9:2 for the active material, binder, conductive additive, buffer components, and dispersant, respectively.[9,28] A total of three 9.5 mm silicon nitride balls were placed in the mixing jar. The slurry was mixed with a planetary ball mill (Fritsch Pulverisette 7 classic line mixer) for 1 hour at 500 rpm.

2.2 Electrochemical Measurements

Coin cells (CR2032, Hohsen Corp.) were assembled using dried Si electrodes (0.50 cm^2 discs) as the negative electrode material and $LiNi_{0.6}Mn_{0.2}Co_{0.2}O_2$ (NMC622, Customcells®, 0.50 cm^2 discs) as the positive electrode unless otherwise stated. Both the negative and the positive electrodes were dried at 100°C, overnight, prior to cell assembly. The cells were balanced with a capacity excess of ~10% for the Si negative electrode, to avoid Li plating. One layer of a 16 mm diameter Celgard 3501 separator was used in each cell. Three different IL electrolytes were

prepared: 3.2 m LiFSI in P_{1222}FSI, 3.2 m LiFSI in trimethyl(isobutyl)phosphonium (P_{111i4})FSI, and 2.0 m LiFSI in methyl(tri-isobutyl)phosphonium ($P_{1i4i4i4}$)FSI (Figs. S1 and S2). Prior to electrolyte preparation, LiFSI and the ILs were dried separately at 50°C under vacuum for 48 hours before mixing. The final water content of the ILs was below 20 ppm as measured by Karl Fischer titration analysis (831 Karl Fisher Coulometer). After drying, the materials were transferred to an Argon-filled glovebox (<1 ppm O_2 and 0 ppm H_2O). The mixtures of the ILs and LiFSI salt were prepared by dissolving appropriate amounts of the salt into the IL. The mixtures were left stirring at 50°C overnight inside the inert-atmosphere glovebox. The three electrolyte have been prepared with the highest concentration possible, close to the LiFSI saturation point in order to investigate the effect of a saturated electrolyte on the electrochemical behavior of the Si/NMC622 full cells. The salt concentration is lower in the case of $P_{1i4i4i4}$FSI ionic liquid compared to the two other systems because 3.2 m LiFSI is beyond the saturation point. A 2.0 m is the highest concentration that could be reached here. The separator was soaked in 25 µL of the electrolyte on a glass microscope slide before placing it in the cell. A total volume of 75 µL of electrolyte was added to cover the separator and the electrodes. One 1 mm spacer and a 1.4 mm spring were used in the assembly. The coin cell was then sealed using a Hohsen coin cell crimper.

After assembly, the cells were placed inside a 50°C oven and allowed to rest for 24 hours prior to cycling. Cycling was performed at 50°C using formation steps of C/40 and C/20. The C-rate for long-term cycling was C/5 with voltage cutoffs at 2.8 and 4.1 V. The transport properties of the the family of IL electrolytes investigated here were investigated separately by previous studies[12,20,29,30] from the group of Forsyth. IL electrolytes usually suffer from low ionic conductivity due to their high viscosity at room temperature. This problem is moreover

exacerbated when electrolyte salts such as $LiPF_6$, LiTFSI, or LiFSI are added. As a result, room-temperature cycling using these electrolytes is typically performed at low C rates up to C/5 due to the poor transport properties of the electrolyte. These drawbacks can be avoided by limiting the salt content to below ~1.2 M and cycling at elevated temperatures of 50−100 °C. Here, with the aim at studying the behavior of highly concentrated electrolyte, in particular with rate capability tests, as well as the formation and evolution of the SEI and the origin of the capacity fading, we decided to maintain a moderately high temperature of 50 °C. Such cycling conditions are similar to those previously used in our previous published works on the subject[12,22] also easing a comparative study. As a point of reference, the ionic conductivity of 3.2 LiFSI in $P_{1222}FSI$ is 0.94 $mS.cm^{-1}$ at room temperature and increases to 2.40 $mS.cm^{-1}$ at 50°C.[12] All the cells have been reproduced at least three times.

2.3 Differential Capacitance Measurements

Differential capacitance (DC) experiments were carried out using a three-electrode set-up inside an Argon-filled glovebox and measurements were performed using a Biologic (SP-200) potentiostat. A glassy carbon (1 mm diameter, eDAQ) working electrode (WE) was chosen to represent the surface of Si. Both materials are semiconductive and have comparable band gaps, i.e. 1.12 eV[31] for Si while a range of ~0.5-2.5 eV[32] has been reported for glassy carbon. The reference electrode was assembled using a silver wire soaked in silver triflate (AgOTf)-IL electrolyte (~0.01 M AgOTf in IL), separated from the bulk electrolyte by a glass frit. Lastly, a platinum wire counter electrode was chosen because of its inert properties. EIS measurements were carried out based on our previous work[22] and the capacitance calculations were adopted from the literature[33].

2.4 SEI Characterization

2.4.1 Transmission Electron Microscopy (TEM)

The cycled Si electrodes were analyzed for elemental composition and imaging using a scanning TEM (STEM), Nant'Themis Z G3 Cs-probe corrected microscope (Thermo Fischer Scientific). The samples were prepared by first scraping the electrodes off their current collector to obtain some samples in the form of powder. This step was performed inside an Argon-filled glovebox. The copper grid (Lacey, 300 mesh) was placed directly onto the scraped-off Si electrode to deposit enough sample for analysis. The copper grids with the samples were then secured in a transfer box (GATAN 648) inside the glovebox and sealed prior to transfer to the microscope. The equipment was operated at 300 kV and equipped with a high-angle annular dark field (HAADF) detector. Elemental maps were acquired in STEM mode using a Super-X emission X-ray spectrometer consisting of four windowless silicon-drift detectors (SDDs), which provides a large collection solid angle of 0.7 srad. For the electrodes measured, this configuration ensured a limited sensitivity to the orientation of the aggregates with respect to the detectors. In order to limit electron beam degradation effects, a low current (70 pA) was used to reduce the electron dose. Pixel sizes of 2-3 nm were chosen. For this same reason, fast frame acquisitions were used (1s per frame) and hundreds of frames were summed for each map. Quantifications performed on the first dozens of frames gave very similar results to those performed on the last dozens of frames, thus proving the reliability of the reported atomic ratios and maps. Regions purely composed of LiF were nevertheless slightly degraded in these conditions, without major implications on the relevance of the maps presented in this manuscript. Atomic percentage quantifications were performed using the Velox 2.14 software and built-in cross sections (Brown-Powell). Pixel averaging was used to improve the reliability of quantification. Spatial resolution of the maps can thus be estimated to be around 8 nm. A "method" was defined

(background, fit, absorption correction, etc.) and systematically used in order to optimize the relative comparison of the various maps and samples.

2.4.2 X-ray Photoelectron Spectroscopy (XPS)

Ex situ XPS analyses of the Si electrodes were performed using a Kratos Axis Nova Instrument. The cycled electrodes were removed from the current collector inside an Argon-filled glovebox. Adhesive conductive carbon tapes were fixed on the XPS sample holder and deposits of the cycled Si electrodes were carefully placed onto the adhesive tape. The sample holder was positioned on the XPS transfer chamber, and it was sealed before the transfer from the glovebox to the XPS machine.

The tube containing the samples was fixed on the XPS instrument and left under vacuum overnight. Upon analysis, the instrument has a base pressure of 5×10^{-10} Torr. The X-ray source was a monochromatic Al Kα (1486.6 eV) operating at 300 W. The probe size, i.e. area under examination, was 0.7 mm x 0.3 mm. A wide range survey spectrum was first acquired with a pass energy of 80 eV. The overall instrumental resolution is 0.9 eV measured on Fermi edge. After obtaining the survey spectra, the pass energy was set to 40 eV for the acquisition of the region spectra for C 1s, O 1s, F 1s, N 1s, Li 1s, Si 2p, S 2p, and P 2p. The overall instrumental resolution was 0.55 eV measured on Fermi edge.

The XPS data was analyzed using the CasaXPS software and using the Shirley background correction. All the spectra were calibrated with respect to C 1s with a binding energy of 285.0 eV. Fitting was performed to identify the different peaks based on their binding energies. Gaussian/Lorentzian (70/30%) line shapes were used to fit the peaks.

2.4.3 Solid State Magic Angle Spinning Nuclear Magnetic Resonance (MAS NMR)

A Bruker 500 MHz Ultrashield spectrometer (B_0 = 11.8 T, Larmor frequencies $\nu_0(^7Li)$ = 194 MHz, $\nu_0(^{19}F)$ = 470 MHz and $\nu_0(^{31}P)$ = 202 MHz) was used for the MAS NMR measurements to monitor the composition of the SEI formed on the surface of Si electrodes after cycling in the various electrolytes. The samples were prepared by recovering the electrodes inside an Argon-filled glovebox. Each cycled electrode was recovered after the end of delithiation without being washed. The recovered powder samples were packed in 2.5 mm zirconia rotors inside an Argon-atmosphere glovebox for ^7Li, ^{19}F, and ^{31}P NMR analyses.

The spinning frequencies were 25 kHz, 23 kHz, and 15 kHz for ^7Li, ^{19}F, and ^{31}P NMR, respectively. The spectra for ^7Li NMR were acquired by employing a single pulse sequence with a recycle time of 40 s. ^{19}F NMR spectra were acquired using a Hahn echo sequence to remove the significant signal contribution coming from the probe. The recycle time was 40 s. Long recycle times or delays were used to ensure full relaxation and quantitative results. All MAS NMR experiments were performed at room temperature.

Fitting of all the spectra was performed using the Dmfit software[34] to deconvolute the peaks. The composition of the detected species was identified based on the chemical shifts of the different resonances observed from the various spectra. The spinning sidebands were also taken into account.[35,36]. Quantitative NMR was also performed by mixing Si with various amounts of LiF to obtain calibration curves which allow absolute quantification of the lithiated and fluorinated components in the samples.[37] Integrated intensities from the ^7Li and ^{19}F NMR combined with these curves allow us calculating the amount of LiF and other lithiated species. All the spectra were normalized to take into account the number of scans, the receiver gain, and the mass of the sample.

3. RESULTS AND DISCUSSION

3.1 Electrochemical Performance in Different Phosphonium IL Electrolytes

Fig. 1 displays the cycling behavior of full Si/NMC622 Li-ion cells in three different phosphonium-based IL electrolytes at 50°C, cycled at a rate of C/5. The corresponding charge-discharge profiles for representative cycles are displayed in Fig. S3-b and S3-c. An almost similar rate of capacity decay upon cycling is observed. However, the cells cycled in P_{1222}FSI-LiFSI and P_{111i4}FSI-LiFSI evidently display higher capacity compared to that cycled in $P_{1i4i4i4}$FSI-LiFSI. Because the difference among these electrolytes is mainly the size of the cation, it can be expected that the observed electrochemical behavior is due to the length of the IL cation alkyl chains.

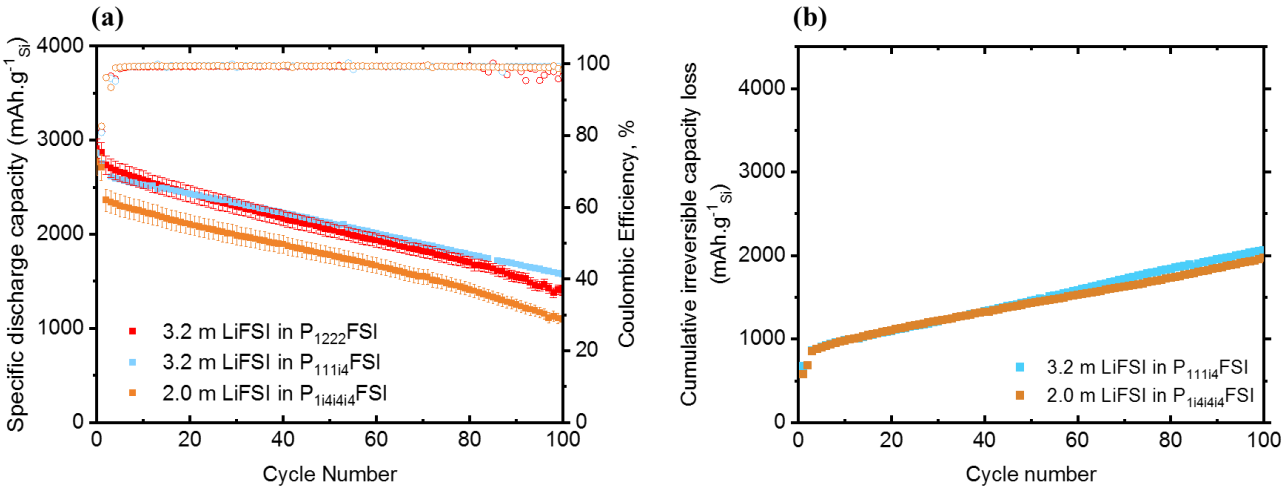

Figure 1. a) Electrochemical performance of Si/NMC622 cells at 50°C showing the Si specific capacity vs. cycle number of the cells cycled in the superconcentrated IL electrolytes and b) cumulative irreversible capacity loss as a function of the cycle number for P_{111i4}FSI-LiFSI and $P_{14i4i4i}$FSI-LiFSI. Specific capacities are given in mAh per gram of silicon (mAh.g $^{-1}_{Si}$)

We have previously [12,22] demonstrated the impact of IL cation nature on the electrochemistry and SEI of Si-based batteries. Here, our results suggest that the size of the IL cation also has a role to

play in the behavior of the batteries. The size of the species making up the electrolyte typically affects the viscosity and ionic conductivity. The influence of the IL cation size is easily demonstrated by rate capability tests to evaluate how the electrolytes can sustain different current densities. Fig. 2 shows that the P_{1222}FSI and P_{111i4}FSI systems exhibit almost similar full cell rate capabilities, sustaining good areal capacities from C/10 up to C/2 at 50°C. This is expected because both electrolytes have approximately the same ionic conductivity (~0.9 mS cm^{-1} at 50°C)[12,20] and viscosity (~100 mPa s at 50°C)[20]. On the other hand, the $P_{1i4i4i4}$FSI-based electrolyte shows poor rate capability even at low cycling rates. The poor rate performance is exacerbated at high rates, e.g. 2C, where the transport of Li ions through the electrolyte becomes very restricted. This can be attributed its lower ionic conductivity and higher viscosity[20] because of the bulky IL cation structure. At first sight, this result appears contradictory with previous studies reported by Hilder et al.[38] and Kerr et al.[39]

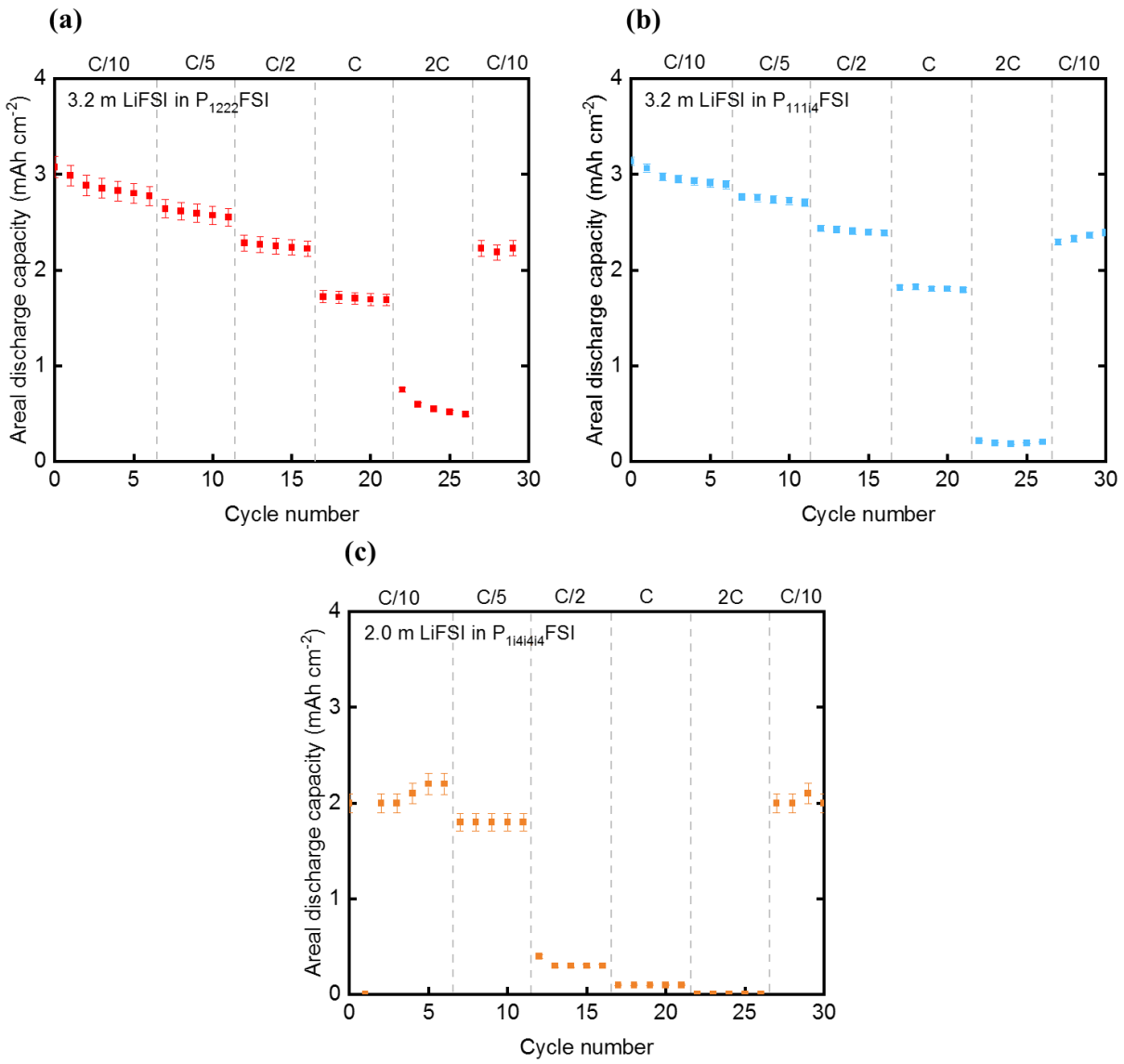

Figure 2. Full-cell rate capability performance of Si negative electrode with NMC622 positive electrode in a) 3.2 m LiFSI in $P_{1222}FSI$, b) 3.2 m LiFSI in $P_{111i4}FSI$, and c) 2.0 m LiFSI in $P_{1i4i4i4}FSI$ at 50°C. Specific capacities are given in mAh per cm^2 of silicon electrode.

While the successful use of $P_{1i4i4i4}FSI$ IL as a battery electrolyte was previously reported on a Na metal system by Hilder et al.[38], Kerr et al.[39] prepared a similarly bulky tetraalkylphosphonium, namely trimethylisobutylphosphonium(P_{1444})-FSI, for Li metal cells but did not succeed in cycling the batteries. In their work with Na metal, Hilder et al. reported a drastic capacity loss for

the cells cycled in highly concentrated (45 mol%) $P_{1i4i4i4}$FSI-NaFSI, with only 11% of its initial capacity remaining after 100 cycles. On the contrary, a stable cycling was achieved with P_{111i4}FSI-NaFSI (42 mol%). The trend observed for the capacity retention aligns with the general trend obtained from this work, where the $P_{1i4i4i4}$FSI system yields a 46% capacity retention after 100 cycles while the P_{1222}FSI and P_{111i4}FSI systems exhibit better capacity retentions of 50% and 60%, respectively (Table 1). In their work, Hilder et al. associated the cycling behavior to the electrochemical impedance spectra of the cells, where the bulky phosphonium system displayed an increasing impedance upon cycling, while the contrary was observed in the small phosphonium system. The Nyquist plots of the Si/NMC622 cells, obtained in a 2-electrode cell configuration and cycled in the various IL electrolytes in this work are presented in Fig. S5. While there is no significant change in the impedance even after 50 cycles, the impedance of the cells cycled in $P_{1i4i4i4}$FSI-LiFSI is larger compared to those cycled in the small phosphonium IL electrolytes, i.e. 150 Ω for $P_{1i4i4i4}$FSI-LiFSI vs. 120 Ω for P_{1222}FSI-LiFSI and 70 Ω for P_{1111i4}FSI-LiFSI after the 50th delithiation. In addition, the electrolyte resistance is considerably larger for $P_{1i4i4i4}$FSI-LiFSI (30 Ω for $P_{1i4i4i4}$FSI-LiFSI vs. 8 Ω for P_{1222}FSI-LiFSI and P_{1111i4}FSI-LiFSI) in agreement with its lower ionic conductivity[20]. The larger impedance in the bulky cation system suggests a more blocking passivation of the electrode surface while more clearly separated semi-circles are observed with respect to the case of smaller phosphonium cations. This second, clearly defined semi-circle, could be assigned either to the formation of a surface film or SEI with different properties, or to a change in the charge transfer process that could be, in turn, linked with a different electrolyte structuration near the electrode surface, which both warrant further investigation. As a result, the structure of the electrolyte components near the electrode surface was studied here using differential capacitance measurements and is discussed in the

succeeding section. Furthermore, the impedance of the full cells cycled in the IL electrolytes appears to be more stable upon cycling compared to those in carbonate electrolytes reported in the literature[40]. This highlights the promising use of IL-based electrolytes in controlling the dynamic nature of the SEI formed on Si electrodes. In fact, the stability of the electrode/electrolyte interfacial resistance points towards the question of the evolution of the electrode/electrolyte interphase in terms of its amount and composition. The characterization of the SEI at the Si electrode is discussed in section 3.3.

Finally, compared to what is reported in the literature with Li-metal batteries[25], the results obtained here with the $P_{1i4i4i4}$-based electrolyte for a Si negative electrode are noticeably superior. These contrasting results may be due to the to the nature of the electrode surface, i.e. metallic or semiconductive, which is worth investigating in future research.

One notable difference between half cell and full cell performance of the Si negative electrode is the faster capacity loss in the latter case. After 100 cycles, the Si electrode cycled in the highly concentrated P_{1222}FSI-LiFSI electrolyte still maintains a capacity of about 80%[12] in the half cell format, while only 50% of the capacity remains in the full Li-ion cell. The stable half cell performance of P_{111i4}FSI-LiFSI are displayed in Fig. S6, which have also been previously reported by Kerr et al.[41] The amount of available Li is usually expected to be responsible for these results since in full Li-ion batteries, the supply of Li is limited and is governed by the positive electrode material. Hence, it becomes more difficult to maintain the performance of the cell as Li ions are consumed in the SEI formation in every cycle or in other parasitic side reactions, resulting in a continuous capacity fade. Many studies[36,42-45] have in fact ascribed the capacity loss in full cells based on Si or Si-graphite negative electrodes and carbonate electrolytes to the exacerbated loss of Li inventory during cycling due to the uncontrollable

growth of the SEI. In addition to the contribution of Si, there are several phenomena happening at the NMC positive electrode that may result in capacity decay. For instance, the dissolution of transition metal ions, e.g. Co, Mn, Ni, from the positive electrode has been frequently reported.[46-50] This may lead to the migration of such ions to the negative electrode, a phenomenon called crosstalk, to participate in the SEI formation. The characterization of the SEI forming at the positive electrode will be also discussed below, in section 3.3.

The first Coulombic Efficiency (CE) of full cells is controlled by the electrode (positive or negative) which has the highest first irreversible capacity loss, hence the lowest first CE. The typical first CE of Si-based electrodes varies from 70 to 85%[51] while Ni-containing positive electrodes have initial CEs ranging from 85-90%[52]. In this study, CEs for the first cycle in half cells were measured in the 85% to 94% range for NMC622 electrode in our IL electrolytes (see Figs. S4c and S4d) while CEs between 81% and 85% were found for Si electrodes (see Table 1), thus indicating that the CE of the first cycle of our full cells is controlled by the Si electrode. The first cycle CE results presented in Table 1 are very promising, indeed very close to the first cycle CE values measured for Si electrode in half cells. The possible contribution of the CEI (Cathode Electrolyte Interphase) at subsequent cycles will be also explored below.

Table 1. First irreversible capacity with the corresponding first Coulombic Efficiency and capacity retention of the Si/NMC622 full cells cycled in the IL electrolytes at 50°C. Specific capacities are given in mAh per gram of silicon ($mAh.g^{-1}_{Si}$)

Electrolyte	1st Irr. Capa. ($mAh\ g^{-1}_{Si}$)	1st Coulombic Efficiency		Capacity retention after 100 cycles
		Full cell	Half cell (Si vs. Li)	
3.2 LiFSI in $P_{1222}FSI$	680	81%	85% (611 $mAh.g^{-1}_{Si}$)	50%

3.2 m LiFSI in $P_{111i4}FSI$	675	81%	83% (650 $mAh.g^{-1}_{Si}$)	60%
2.0 m LiFSI in $P_{1i4i4i4}FSI$	580	83%	81%	46%

3.2 Near-Electrode Structure of the IL Electrolyte Components

Differential capacitance (DC) measurements have been widely employed in supercapacitors to obtain information regarding the structure of the electrical double layer (EDL) of various electrolytes and assess their capability to store energy non-Faradaically. This concept is applied here to provide similar information at the electrode/IL electrolyte interface which can be useful in explaining the observed electrochemical behavior. A glassy carbon electrode was used to represent the Si electrode by virtue of their similar semiconductive nature. The same setup was previously[22] used for a similar type of investigation in which the results were validated by computational methods. The DC profile of $P_{1i4i4i4}FSI$-LiFSI produces a U-like profile as shown in Fig 3. This profile is typical of those performed on glassy carbon electrodes[53,54] and are also similar to what we reported in the case of $P_{1222}FSI$ and C_3mpyrFSI-based electrolytes[22]. The addition of Li salt strongly affects the capacitance especially on the FSI-dominated region, i.e. more positive polarization. The capacitance gain in the highly concentrated system compared to the neat as seen in Fig. 3a is attributed to the high Li concentration that leads to more charge per volume, hence the higher capacitance at the electrode.

The influence of the IL cation size is demonstrated by comparing the DC profile of $P_{1i4i4i4}FSI$ to that of $P_{1222}FSI$ (Figs. 3b and 3c). The bulkier IL with longer alkyl chain length has a lower capacitance, regardless of salt content, i.e. neat or with LiFSI salt. This is because of its thicker double layer, which is inversely proportional to the capacitance of the system. The structure of the double layer, hence, the capacitance, can be linked to the packing of the ions with respect to

the electrode surface. The effect of cation size has already been explored a long time ago. Lockett et al.[55] observed a similar pattern for 1-methyl-3-ethylimidazolium chloride (emimCl), 1-methyl-3-butylimidazolium chloride (bmimCl), and 1-methyl-3-hexylimidazolium chloride (hmimCl), where the capacitance is increasing in the order: hmimCl, bmimCl, and emimCl. In this previous work, the IL cation size was also observed to influence the interaction of FSI anions with the electrode. A similar effect can thus be expected here with an altered interaction between FSI anions and the surface of the electrode depending on the different packing of the IL cations e.g. the small P_{1222}^{+} or the bulky $P_{1i4i4i4}^{+}$. A Further investigation of the cyclic voltammetry (CV) presented in Fig. S7 reveals one notable feature upon careful examination of the $P_{1i4i4i4}$FSI CV curve. A small cathodic hump appears at approximately -1.36 V vs. $Fc|Fc^{+}$ which is assigned to the decomposition of FSI^{-} anions[56]. The result is consistent with the previous capacitance measurements and it is inferred here that the bulky nature of the $P_{1i4i4i4}^{+}$ cation which packs poorly based on its lower capacitance provides increased access to the FSI anions to reach the electrode and potentially to undergo decomposition. In contrast, the absence of the said feature in the P_{1222}FSI system (Fig. S7) could indicate a more efficient and compact packing of the IL cations at the electrode surface, which diminishes FSI anions interaction with the electrode. This very important result suggests that reactions at the electrode/electrolyte interface will be different and may lead to SEIs with different compositions and properties, depending on the size of the IL cation, its packing close to the surface controlling the interaction between FSI anions and silicon surface. In the following sections, we explore the SEI composition for the two IL electrolytes, based on the small P_{1222}^{+} and bulky $P_{1i4i4i4}^{+}$ cations.

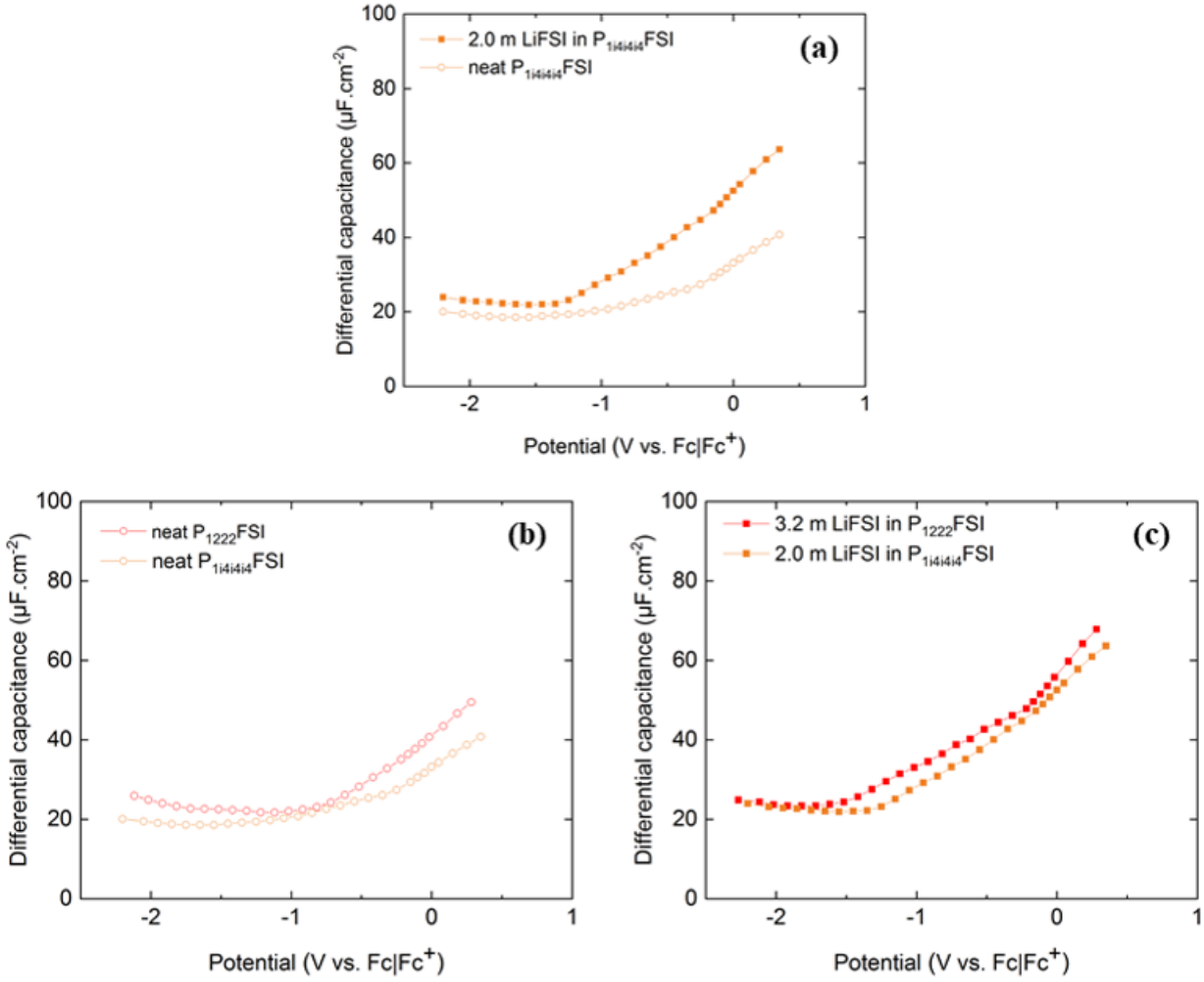

Figure 3. Differential capacitance curves of a) neat $P_{1i4i4i4}FSI$ vs. $P_{1i4i4i4}FSI$-LiFSI b) neat $P_{1i4i4i4}FSI$ vs. neat $P_{1222}FSI$, and c) $P_{1i4i4i4}FSI$-LiFSI vs. $P_{1222}FSI$-LiFSI electrolytes measured at 55°C with a GC working electrode.

3.3 SEI Characterization

The cycled electrodes were initially analyzed with TEM to obtain information about the microstructure of the Si nanoparticles after extended cycling. From the high-angle annular dark-

field (HAADF) images in Figs. 4a to 4b, it appears that the Si particles are not severely broken down after 100 cycles in the various electrolytes investigated. This result is in contrast with the state of the electrodes after the same extent of cycling in half-cell configuration[22], where the particles were evidently pulverized (Fig. S8). The reason for this is that the Si electrodes were cycled without capacity limitation in half cells, utilizing all the available Si for lithiation (and delithiation). In such case, the volumetric expansion is maximized and leads to the ultimate breakdown of the particles. The full capacity is particularly utilized in the early stages of cycling, giving above 3000 $mAh.g^{-1}_{Si}$. In the case of full Li-ion cells (negative electrode is slightly in excess), the charging (lithiation) is limited by the available Li at the positive electrode which does not take up all the available Si. As seen in Fig. 1, the full capacity of Si, i.e. ~ 3579 $mAh.g^{-1}_{Si}$, is not attained in the first cycle and conceivably in the succeeding cycles. This result is consistent with the Si particles having undergone a considerably reduced mechanical stress upon cycling and that after repeated lithiation and delithiation, the well-documented pulverization process of the Si particles has not occurred or has occurred to a much lesser extent.

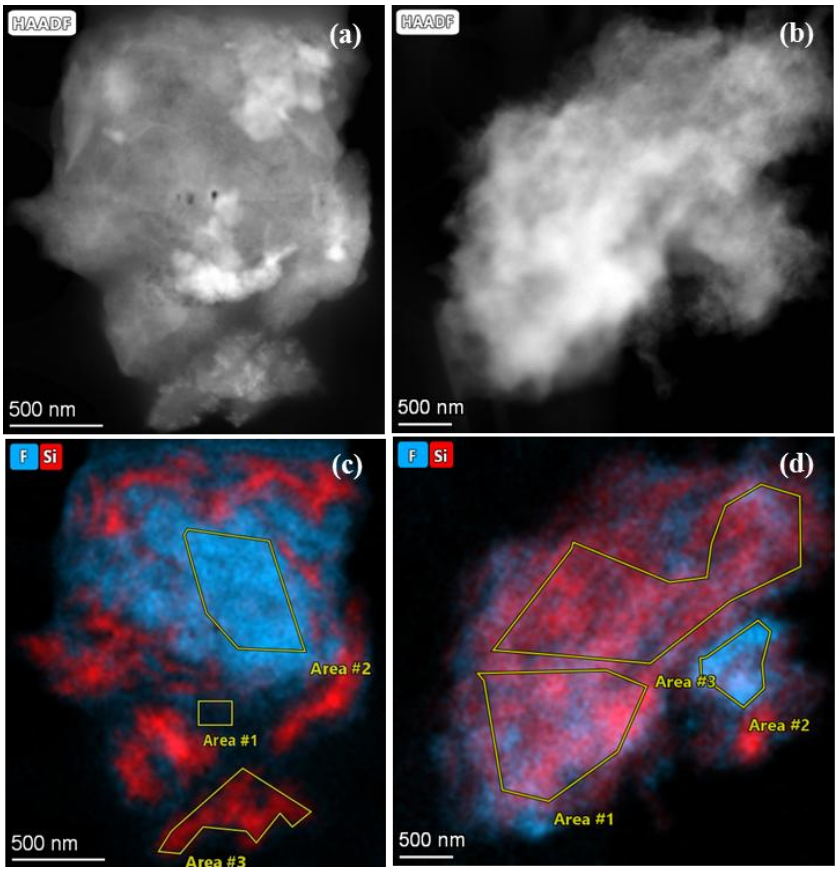

Figure 4. TEM images of the Si electrode after 100th delithiation in STEM-HAADF mode (a) and STEM-EDX mode (c) for $P_{111i4}FSI$ with 3.2 m LiFSI and STEM-HAADF mode (b) and STEM-EDX mode (d) for $P_{1i4i4i4}FSI$ with 2.0 m LiFSI. *(Areas delimited in yellow correspond to the regions analyzed for elemental quantification in Table S2)*

STEM-EDX analysis focusing on Si element (Fig. 4c and 4d), appearing in red confirms clearly that the complete pulverization of Si towards filament-like bundles of nano-particles, as observed in the case of half-cells (Fig. S8) and in other studies[57], has not occurred here. STEM-EDX analysis was also performed to reveal the interfacial makeup of the Si electrodes after cycling. Figs. 4c to 4d focus on F and Si elements to examine how the SEI, which typically contains F stemming from FSI^- degradation, is distributed throughout the Si particles. The presence of other elements (oxygen, phosphorus, sulfur) was also examined and is presented in Fig. S9. As can be

observed, the SEI seems to uniformly cover the Si particles and appears to contain breakdown products of IL anions, as in the case of half-cells, since the expected N:S:F and O:S ratios of the non-degraded FSI anion are not met (Table S2). Scans for positive electrode elements, e.g. Mn, Co, Ni, were performed to investigate the occurrence of crosstalk phenomenon but no sign of such elements were detected on the negative electrode. The SEI composition is then further investigated quantitatively with XPS and MAS NMR in the succeeding paragraphs.

XPS confirmed the chemical composition of the interphase formed on the Si electrode surface after cycling in the IL electrolytes (Figs. 5a and 5b). The F 1s, N 1s, and S 2p spectra reveal the presence of both intact and decomposed LiFSI. The pristine LiFSI peaks rise at about 687.4 eV, 399.4 eV, and 169.5 eV[58] in the F 1s, N 1s, and S 2p spectra, respectively. The Li salt decomposition results mainly in LiF (684.6 eV in F 1s)[58,59] and S=O groups[58], e.g. $-SO_4^{2-}$ (168.2 eV for P_{111i4}FSI and 168.3 eV for $P_{1i4i4i4}$FSI in S $2p_{3/2}$)[59] and SO_3^{2-} (167.0 eV for P_{111i4}FSI and 166.9 eV for $P_{1i4i4i4}$FSI in S $2p_{3/2}$)[59]. The $-SO_4^{2-}$ group could be assigned to Li_2SO_4. The S 2p spectrum of the electrode cycled in P_{111i4}FSI-LiFSI also indicates the formation of Li_xS or Li_2S, corresponding to the minor signal within the range of 160-165 eV[60]. The possibility of X-ray beam-induced salt degradation[61] can be ruled out because no signs of pristine phosphonium cation degradation was observed, i.e. beam damage (if present) should affect both the IL cation and anion.

The P 2p spectra (rightmost figures in Figs. 5a and 5b) confirm the stability of both the small and bulky phosphonium cations even after the 100th delithiation. The signals at 132.7 eV ($2p_{3/2}$) and 133.6 eV ($2p_{1/2}$) correspond to the intact P_{111i4}^+ cation, whereas the P 2p peaks for the unaltered $P_{1i4i4i4}^+$ cation appear at 132.6 eV ($2p_{3/2}$) and 133.5 eV ($2p_{1/2}$).

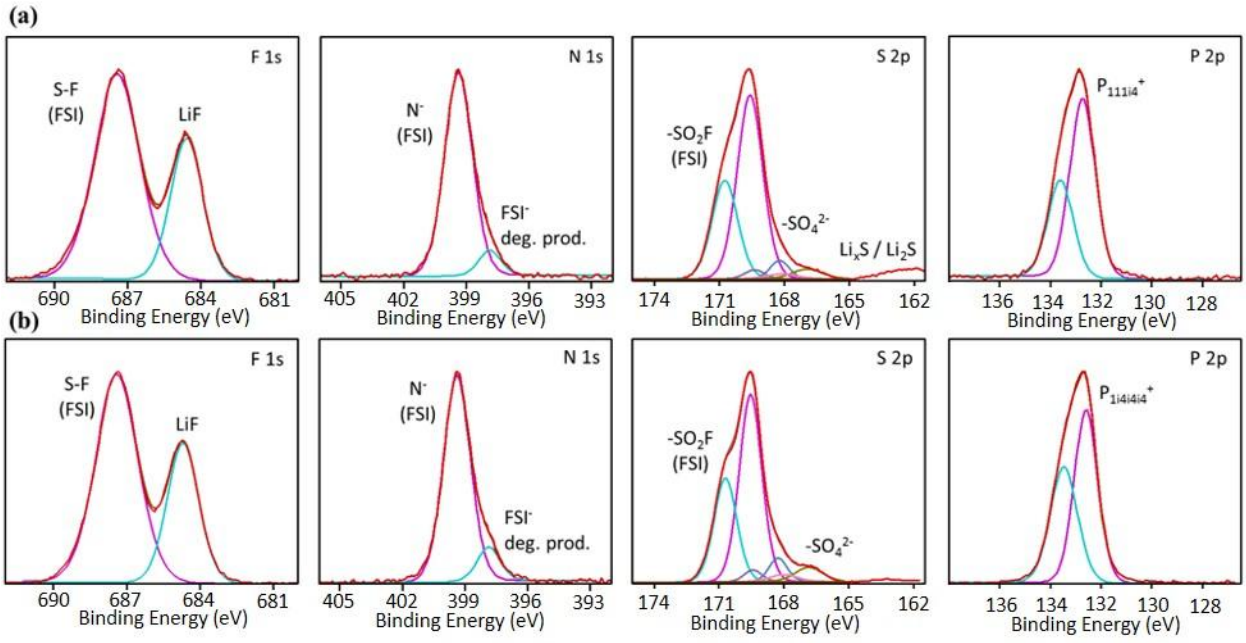

Figure 5. XPS F1s, N 1s, S 2p, and P 2p spectra of the Si electrodes after the 100th delithiation in a) P_{111i4}FSI with 3.2 m LiFSI and b) $P_{1i4i4i4}$FSI with 2.0 m LiFSI.

Ex situ MAS NMR was used to obtain both qualitative[12,30,36] and quantitative[37] information about the composition of the SEI layer that formed from the interaction of the electrodes with the IL electrolytes. The ^{31}P MAS NMR spectra obtained after 100 cycles and illustrated in Fig. S10 confirm the stability of the phosphonium cations in full cells. The main resonances arising at approximately 22 ppm, 26 ppm, and 35 ppm[22] for the Si electrodes cycled in the P_{111i4}FSI-, $P_{1i4i4i4}$FSI-, and P_{1222}FSI-based electrolytes, respectively, is assigned to a non-degraded IL which verifies that the cation remains intact after extended cycling. The said resonances have a sharp component that corresponds to more mobile species and a broad component that indicates the presence of less mobile species that can be reasonably assigned to trapped IL cations

incorporated into the SEI layer or less mobile IL cations near the electrode surface. The ^{31}P NMR spectra of the positive electrode (Fig. S13) also indicate the presence of unaltered phosphonium cations. However, their intensity is noticeably less than those in the negative electrode, e.g. ~ 3x less based on integrated intensity for the P_{111i4}FSI-LiFSI system. This suggests a possible preferential involvement of IL components in the SEI formation on the negative electrode or a sign of a thinner CEI on the positive electrode side.[62]

Figs. 6a and 6b present the ^{7}Li NMR spectra of the Si electrodes cycled in the phosphonium-based electrolytes and stopped at the end of the 5th and 100th delithiation. The normalized integrated intensities show one major resonance at about 0 ppm which is typically associated with diamagnetic Li species. Moreover, the chemical shift is leaning towards more negative values, indicating contributions from fluorinated products.[36] The signal consists in a prominent broad component and a sharp constituent in most cases. The broad contribution may contain several overlapping peaks from various lithiated species which may include LiF, Li_2O, Li_2S, LiOH, Li_4SiO_4, Li_2SO_4, and LiFSI.[30,36,63-66] The ^{19}F NMR spectra in Fig. S11 confirm the presence of LiFSI and LiF, which appear at approximately 54 ppm and -204 ppm, respectively. The ^{19}F LiFSI signal contains sharp components that are attributed to mobile species and broad components that are assigned to confined products. On the other hand, the LiF resonance only exhibits a broad profile which indicates that it is indeed embedded within the SEI.

The normalized integrated intensities as seen in the ^{7}Li spectra in Figs. 6a to 6b suggest that there is no significant change from the 5th until the 100th delithiation in either the small or bulky phosphonium-based electrolyte. The same results can be deduced from the corresponding ^{19}F spectra (Fig. S11). This result is important as it suggests a more stable SEI, for instance, compared to the SEI formed in half cells where the intensity of the NMR spectra clearly

increases upon cycling (Fig. S12). From the spectra alone, it seems that the film making up the SEI of the Si electrode is similar in half and full cells. However, quantitative analysis of the species, i.e. LiF and other lithiated products, using combined ^{7}Li and ^{19}F NMR[37] reveals important differences between the IL electrolytes and between the two cell configurations as elucidated in the following discussions. We refer here to other lithiated products in the case of the typical diamagnetic lithiated species, apart from LiF, forming from the salt degradation and having very similar ^{7}Li chemical shifts, in the -2 to 3 ppm, such as LiFSI, LiOH, Li_2S and Li_4SiO_4, already observed in our previous work[12,22]. Their very similar ^{7}Li NMR chemical shifts prevent any accurate discrimination and quantification. On the contrary, the very specific ^{19}F chemical shift for LiF allows a much easier and reliable spectral separation from other species. The quantities of the SEI products derived from calibration curves[22] and summarized in Figs. 6c and 6d highlight the comparable amount of LiF (1.2 µmol.$mg^{-1}_{electrode}$) as well as Li found in other lithiated species altogether (4.8-5.0 µmol.$mg^{-1}_{electrode}$) after 5 and after 100 cycles in the case of the P_{111i4}FSI with 3.2 m LiFSI electrolyte. This surprising result confirms an extremely stable SEI at least from the LiF and detected Li point of view, which is supported by the very stable impedance as observed in the Nyquist plot (Fig. S5). An almost similar behavior is observed for the $P_{1i4i4i4}$FSI with 2.0 m LiFSI electrolyte, with a slight evolution from 0.6 µmol. $mg^{-1}_{electrode}$ to 1.4 µmol. $mg^{-1}_{electrode}$ of LiF and 5.2 µmol. $mg^{-1}_{electrode}$ to 5.9 µmol. $mg^{-1}_{electrode}$ of Li involved in species other than LiF. On the contrary, in the case of half cells, the amount of LiF and other lithiated components from the 10th to the 100th delithiation increased from 3.5 to 5.5 and 1.0 to 5.9 µmol. $mg^{-1}_{electrode}$, respectively (Fig. S12).

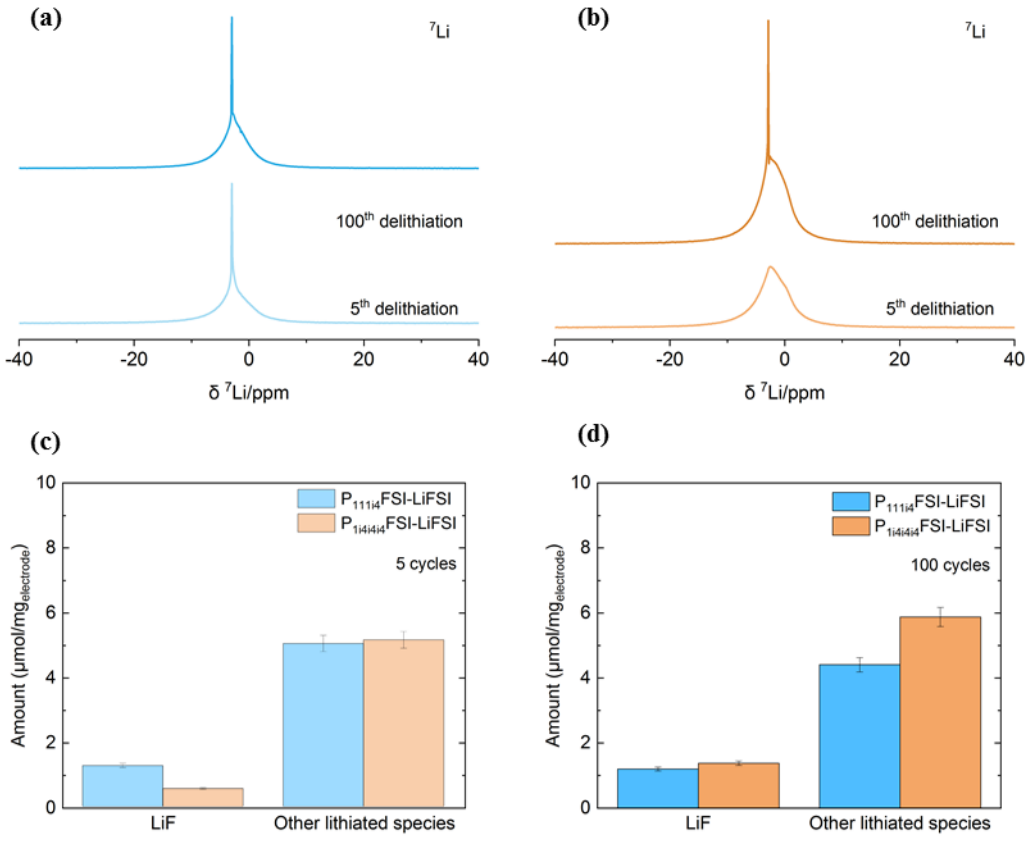

Figure 6. ^{7}Li MAS NMR spectra of the Si electrodes upon cycling in a) $P_{111i4}FSI$ with 3.2 m LiFSI and b) $P_{1i4i4i4}FSI$ with 2.0 m LiFSI; Amounts of LiF and other lithiated products obtained from ^{7}Li and ^{19}F MAS NMR spectra of the Si negative electrodes after c) 5 cycles and d) 100 cycles in the superconcentrated IL electrolytes. Amounts of LiF and other lithiated products are given in μmol per milligram of electrode.

A plot of the cumulative irreversible capacity loss (CICL) was generated (Fig. 1b) to check whether the evolution of the capacity loss is consistent with the MAS NMR quantification of Li ions trapped in the SEI. As can be seen, the steady increase in CICL does not correlate with the stable SEI composition upon cycling as observed in the case of the IL electrolytes from the 5th to

the 100^{th} delithiation. This result indicates that the primary cause of the capacity fading observed in the case of the full-cells, cycled with a superconcentrated IL-based electrolyte, is not the consumption of Li ions necessary to form the SEI.

A first observation concerning the overall similar amount of Li detected by MAS NMR in the SEI at different stages of the cycling indicates that the amount of Li involved in the SEI does not evolve significantly between the 5^{th} and the 100^{th} cycle. In addition, the comparison of the quantities of the SEI products presented in Figs. 6c, 6d and Fig. S12 points towards the lower amount of Li ions involved in parasitic reactions creating the SEI at the surface of Si particles in the case of the full cell configuration after 100 cycles. Concerning the Si electrode side, 5.5 $\mu mol.mg^{-1}_{electrode}$ and 5.9 $\mu mol.mg^{-1}_{electrode}$ (total of 11.4 $\mu mol.mg^{-1}_{electrode}$) of Li are consumed in half cell configuration to create LiF and other lithiated species, respectively. For the full cell configuration at the Si side, 1.2 $\mu mol.mg^{-1}_{electrode}$ and 4.8 $\mu mol.mg^{-1}_{electrode}$ (total of 6 $\mu mol.mg^{-1}_{electrode}$) of Li are consumed to create LiF and other lithiated species, respectively. The amount of Li consumed in parasitic reactions at the Si electrode appears to be lower by a factor of approximately 2 for the full cell configuration compared to the half cell configuration. Moreover, the amount of Li consumed in parasitic reactions at the positive NMC side appears quite negligible, i.e. 0.7 $\mu mol.mg^{-1}$ (3.2 m LiFSI in $P_{111i4}FSI$) and 0.4 $\mu mol.mg^{-1}$ (2.0 m LiFSI in $P_{1i4i4i4}FSI$) after the 100^{th} delithiation, considering that the total available Li from NMC is 10.3 $\mu mol.mg^{-1}_{NMC}$. These results indicate that the steeper capacity fading observed in the case of the full-cell configuration cannot be attributed to a continuous consumption of the limited amount of initially available Li for the positive NMC electrode.

Discussion:

The above characterization results presented the full cell performance of Si-based Li-ion batteries as well as the characteristics of the formed interphase and the evolution of the Si particles. We showed, from MAS NMR quantification, that the consumption of available/cyclable Li^+ ions to form the passivation layers on negative and positive electrodes cannot explain the continuous capacity fading observed upon the cycling of the full cells. The first striking result here is the very stable amount of LiF and other lithiated species (assigned to LiFSI, LiOH, Li_2S and Li_4SiO_4 from XPS analyses) deduced from quantitative ^7Li and ^{19}F MAS NMR measurements. The scenario of SEI evolution is already different from that in half cell configuration, considering the same silicon-based electrode and similar phosphonium-based IL electrolytes[22]. In this latter case, although the overall order of magnitude of the amount of both LiF and other lithiated species (also assigned to LiFSI, LiOH, Li_2S and Li_4SiO_4 from XPS analyses) remains similar to that detected for the full cell configuration, a clear increase is clearly detected for the half cell configuration, as explained in details in the above section. The SEI formation and evolution in IL electrolytes are however very different from what is usually observed for carbonate-based electrolytes[67] When carbonate-based electrolytes are used, lithiated organic species such as alkyl-carbonates and semi-carbonates are typically found[68] in the outer part of the SEI, covering usually inorganic lithiated species such as Li_2CO_3 and LiF. A further comparison from the point of view of SEI species amount, as quantified by MAS NMR, indicates that twice the amount of LiF can be expected for a LP30 + 10 wt% FEC electrolyte after 100 cycles[22] when comparing similar silicon electrodes cycled in half cell configuration. Moreover, whereas decomposition products stemming from the degradation of carbonate solvents are not present in the SEI when IL electrolytes are used (simply because there is no source of such carbonates), the amount of Li involved in organic lithiated species can reach up to

10 or 15 times that of LiF[65]. This significant consumption of cyclable Li has typically drastic consequences in full cell configuration. Moreover, it has been also shown, using ex situ XPS and STEM-EELS on silicon electrodes cycled in full cell configuration[36], that the degradation of carbonate solvents does not stop when all the cyclable Li, available from the positive electrode material, has been consumed. This leads to the formation of non-lithiated organic carbonates species that can be observed on the outer part of the SEI. Again, these non lithiated organic carbonates are obviously not present in the SEI formed when IL electrolytes are used. Scenarii of SEI formation and evolution appear then extremely different between IL and carbonate –based electrolytes. While the significant consumption of cyclable Li in full cell using carbonate electrolytes can usually explain the observed capacity fading upon cycling, such an explanation does not seem to apply in the case of the IL systems studied here since the capacity fading cannot be correlated with a growth of the SEI.

We will discuss now, the possible reasons of the steeper capacity fading in full cell. It appears that the gradual but steeper capacity decay in full cells could be due to one of -or the combined effects of- several phenomena:

i) The breakdown of the Si particles that constantly creates a dynamic SEI:

The breakdown of the particles is less severe compared to the case of half cells. While this process leads to a lesser extent of pulverization of the Si particles and lower the quantity of fresh Si surface exposed to the electrolyte at each cycle, the hindering of the pulverization of Si particles might also lead to a lower porosity of the electrode.

ii) Thickness of the SEI.

A thicker SEI could in fact, clog the intrinsic porosity of the electrode and hinder the electrolyte supply through the tortuous porosity in parts of the electrode. According to the electrochemical performance in full cell configuration presented in Fig. 1, the Si electrode delivers approximately 70% of its full capacity (estimated from the first delithiation capacity), indicating that the full capacity is not utilized. As seen from the less severe disintegration of the Si particles in TEM images after the extended full-cell cycling, it is then reasonable to consider that a more restricted surface of fresh Si is created to be exposed to the electrolyte at each cycle. However, the overall amount of Li trapped in species forming the SEI at the surface of the Si particles after 100 cycles for the full cell is approximatively twice lower than that for the half cell. In fact, only the amount of LiF seems to be lower in the case of the full cell configuration, resulting in a 1.8 ratio for the overall amount of Li trapped in decomposition species in the SEI between half cell and full cell configuration. It is not possible to evaluate accurately the total surface created after the pulverization process of the Si particles after 100 cycles. The less pulverized state of Si particles in full cells compared to half cells creates much less surface area in the former case, hence a thicker SEI could be expected to form in the full cell configuration. However, the stable EIS between the 5^{th} and 100^{th} cycles does not appear to be consistent with this scenario, unless entire regions of the Si negative electrode are insulated from the ionic percolating network, explaining both the capacity fading and the stable EIS measurements. Nevertheless, at this stage, no straightforward link between the stable EIS and the quite linear evolution of the capacity decay could be found.

iii) Loss of electronic percolation within the electrode architecture

Another hypothesis, also involving the insulation of entire regions of the Si negative electrode implies the loss of electronic percolation. In that case, initial electronic contacts provided by the carbon conductive agent may be lost upon the unavoidable movements and rearrangements of Si particles that still exists although to a much lesser extent compared to the case of half-cells. While the thorough pulverization of Si particles could help in a better redistribution of carbon particles to maintain the electronic percolation, the less intense mechanical strains endured in the case of the full cell combined with a stable SEI could lead to a loss of electronic contact points between particles and insulate electronically an entire region of the Si negative electrode, also explaining the capacity fading and stable impedance upon cycling.

iv) Lithium metal electrode volume variation

On the one hand, the massive volume change of the Li metal[69,70] negative electrode at each cycle probably leads to an additional cell internal pressure and may also contribute to the exacerbated fracturing of the Si particles in the case of half cell. Furthermore, Li metal will dissolve and move back and forth upon cycling and will accompany the Si expansion/contraction. On the other hand, the NMC622 positive electrode material in the case of Si/NMC622 full cell does not undergo significant volume change and the internal pressure in the cell is driven by the changes of the Si electrode volume. This could lead to much greater pressure variations upon cycling between the charged and discharged states of the Si electrode in the case of full-cell. Such phenomenon, which remains to be investigated, could contribute to the more rapid capacity fade as well.

Additional experiments with further in-depth characterization are needed to verify the validity of the above points and discriminate the possibility of active mass disconnection from the

percolating network from other reasons that could explain the capacity fading. It appears nevertheless that neither an extensive Li^+ consumption nor the uncontrolled formation of blocking electrode/electrolyte interphases are the cause for capacity fading in full-cell configuration, cycled with superconcentrated IL-based electrolytes. The characterization of cycled electrodes rather points towards mechanical reasons, complete disconnection of part of the electrode, or internal mechanical stress, to explain the progressive capacity fading in full cell configuration.

Concerning the differences in composition of the SEI with respect to the cell configuration, a second observation concerning the quantities of the SEI products presented in Figs. 6c and 6d is the significantly less amount of LiF compared to the other lithiated species. Comparing the cases of half vs. full cells, the amount of Li involved in species other than LiF is quite similar after 100 cycles (5.9 $\mu mol.mg^{-1}_{electrode}$ in the case of half cell and 4.8 $\mu mol.mg^{-1}_{electrode}$ in the case of full cell). However, the amount of detected LiF is significantly varying from 1.2 $\mu mol.mg^{-1}$ in the case of P_{111i4} system in full-cell configuration to 5.5 $\mu mol.mg^{-1}_{electrode}$ in the case of the P_{1222} system in half-cell configuration. We considered here the two phosphonium cations to be equivalent in terms of size and the corresponding electrolytes to display similar intrinsic transport and viscosity properties and to lead to equivalent electrochemical performance. It seems therefore that such a difference in terms of LiF amount may come from the cell format itself. In fact, this result indicates a lower extent of the decomposition of the electrolyte from its interaction with the Si electrode in full cells. This, again, can be due to the more restricted use of the Si particles during cycling. The less severe particle breakdown compared to half cells creates fewer fresh surfaces during cycling that serve as potential sites for electrolyte decomposition. Furthermore, the typical defluorination of FSI^- anions can rapidly lose fluorine which can react

with the infinitely available Li in the case of half cells to form more LiF. Moreover, the reduction cutoff potential reaches 0.01 V in half cells, when the Si electrode is cycled versus Li metal, while the reduction potential of Si in a full Li-ion batteries is most probably higher (lower cutoff potential for Si vs. NMC622 is 2.8 V). In this work, full cells were cycled in a 2-electrode configuration and the determination of the exact potential experienced by the Si negative electrode would require the use of 3-electrode cells. Nevertheless, considering that for the first cycle, only 70% of the Si capacity is delivered, it is reasonable to consider that the full lithiation of Si is not completed and a more positive potential is reached at the end of reduction. This difference in potential might in fact limit the extent of degradation reactions and explain an overall lower amount of LiF.

We are considering now the influence of the IL cation size on the SEI composition: while the quantification of the detected SEI products confirmed that their amounts do not change drastically from the 5^{th} to the 100^{th} cycle, a slight difference in the relative amount of LiF/other lithiated species can be observed for the small and bulky phosphonium systems. For example, the amount of LiF, 1.2 $\mu mol.mg^{-1}_{electrode}$, in the electrode exposed to P_{111i4}FSI-LiFSI electrolyte remains the same after 100^{th} delithiation. However, a slight increase of LiF from 0.6 to 1.4 $\mu mol.mg^{-1}_{electrode}$ is obtained for the $P_{1i4i4i4}$FSI-LiFSI. The explanation of such a different behavior between the two appears to lie in the different packing of IL cations as deduced from differential capacitance experiments (see section 3.2). The more compact packing of the smaller phosphonium IL cations near the electrode seems to hinder or reduce the access of FSI^- anions to the surface, whereas the slightly looser structure of the bulky phosphonium allows more FSI^- anions to reach the electrode and participate in the formation of an increased amount of LiF compared to the case of the smaller phosphonium. This particular result further strengthens the

hypothesis that the other lithiated components are most likely residual or trapped LiFSI[22]. These findings, along with the lower conductivity of the $P_{1i4i4i4}$–based electrolyte, are in agreement with the observed electrochemical performance, where the electrolytes containing small phosphonium cations displayed better cycling behavior and smaller impedance compared to those with the larger phosphonium. The same trend is found for the other lithiated products, but the difference is nearly negligible or within the error of the measurements. Overall, the total Li amount detected after 5 cycles is larger in the case of the short P_{111i4} phosphonium-containing electrolyte, due to a slightly larger amount of LiF. An exact inventory of the lost Li ions and concomitantly consumed electrons in degradation reactions is delicate to perform here without taking into account the Li ions trapped at the positive electrode side but this result appears to be in line with the larger irreversible capacity measured at the very beginning of cycling for the short P_{111i4} phosphonium-based electrolyte (675 mAh.g^{-1}_{Si} and 580 mAh g^{-1}_{Si} for the 1st cycle for P_{111i4} and $P_{1i4i4i4}$ systems, respectively).

4. CONCLUSIONS

In this work, the full cell performance of Si negative electrode was linked to the formed interphase using a combination of qualitative and quantitative ex situ techniques such as TEM / STEM-EDX, XPS, EIS, and MAS NMR. Whereas the diminishing Li inventory upon cycling upon which the lost Li is incorporated in the SEI formation after each cycle is usually the main cause of capacity fading when full cells and half cells are compared, the overall similar amounts of Li detected by MAS NMR in the SEI at different stages of the cycling of the full cells (5th and 100th cycles) at the surface of the Si electrodes lead us to rule this explanation out in the case of IL-based electrolytes. Moreover, Li quantification using ^{7}Li MAS NMR indicated that the amount of Li trapped at the positive electrode side is negligible and is therefore not responsible

either for the observed progressive capacity fading. Moreover, the absence of transition metals (from the positive electrode) on the Si electrode surface indicates that crosstalk does not take place during cycling. IL electrolytes, especially based on phosphonium cations appear here as extremely efficient to control and master the composition and properties of the SEI at the surface of the Si electrode. Nevertheless, replacing carbonate electrolytes with IL-based ones introduces an additional parameter to be taken into account: the structuration of IL ions near the surface of the electrode appears to play a significant role, in terms of the extent of LiFSI degradation and relative amount of LiF. Changing the size of the IL cation appears also as a way to modify or alter this structuration. As deduced from the capacitance measurements, the somewhat looser packing of the bulky $P_{1i4i4i4}$ IL cation near the surface of the electrode permits a better access of the FSI^- anion to the silicon surface and lead to an exacerbated decomposition, visible on the cyclic voltammetry and confirmed by ^{7}Li MAS NMR quantification. Capacitance measurements appear then here as a quite appropriate method to access fine and subtle information permitting to link the different packing of species near the surface of the electrode with the reactions of SEI formation and evolution.

Finally, the gradual but steeper capacity decay in full cells could be due to the combined effects of the following phenomena: (i) the hindering of the pulverization of Si particles might lead to a lower porosity of the electrode. (ii) the progressive disconnection of active material from the ionic and/or electronic percolation network. Considering the lesser extend of Si particles breakdown, a thicker SEI could be expected. Such an SEI could also clog the intrinsic porosity of the electrode and block the electrolyte supply through the tortuous porosity in parts of the electrode. Moreover, the combination of this extremely stable SEI at the surface of the Si particles and the less exacerbated movements/rearrangements/partial breakdown of Si particles,

preventing intra-electrode components redistribution, could lead to electronic contact loss between Si particles. Both hypotheses would lead to progressively insulate, ionically or electronically, entire regions of the Si negative electrode explaining the capacity fading. Nevertheless, this may not be reflected in the stable Nyquist diagrams. (iii) lithium metal electrode volume variation.

Further work is obviously needed and underway to investigate these hypotheses in particular the impact of an electrochemical cycling of Si electrodes in half cell configuration, with limited capacity to reduce the mechanical stress undergone by Si particles as well as the possibility of actual disconnection of entire parts of the electrode. Overall, our findings in this work provide a new interpretation and perspective to the capacity fading in full cells which is traditionally linked to the loss of Li inventory but appear here to be linked to more mechanical reasons.

AUTHOR INFORMATION

Corresponding Authors

*E-mail: nicolas-dupre@cnrs-imn.fr (N.D.), khryslyn.arano@gmail.com (K.A.)

Author Contributions

Khryslyn Araño (K.A.) : experimental investigation, data analysis, manuscript writing, editing and revision. SEM imaging. Nicolas Gautier (N.G.): TEM experiments. Robert Kerr (R.K.): scientific discussion, manuscript editing. Bernard Lestriez (B.L.): project conception, scientific discussion, manuscript editing. Jean Le Bideau (J.LB): project conception, scientific discussion, manuscript editing. Patrick C. Howlett (P.C.H.): project conception, scientific discussion, manuscript editing. Dominique Guyomard (D.G.): project conception, scientific discussion, manuscript editing and revision. Maria Forsyth (M.F.): project conception, scientific discussion,

manuscript editing. Nicolas Dupré (N.D.): project conception, scientific discussion, MAS-NMR experiments and data analysis, TEM sample preparation, manuscript editing and revision.

ORCID

Nicolas Dupré : 0000-0002-0687-9357

Maria Forsyth : 0000-0002-4273-8105

Patrick C. Howlett : 0000-0002-2151-2932

Bernard Lestriez : 0000-0002-6579-5516

Jean Le Bideau : 0000-0003-3959-3694

Robert Kerr : 0000-0001-7499-3920

Dominique Guyomard : 0000-0001-7801-8129

Nicolas Gautier : 0000-0002-0421-9582

NOTES

The authors declare no competing financial interest.

SUPPORTING INFORMATION

-Chemical Structure of the Ionic Liquids
-Electrochemical cycling of full cells – Voltage-composition profiles
-Electrochemical Impedance Spectroscopy
-Half Cell Performance of Si in IL Electrolytes
-Cyclic Voltammetry
-TEM-EDX
-MAS NMR: Si Electrode

-MAS NMR: Positive Electrode

-References

FUNDING SOURCES

K. A. received funding from the French Agence de l'Environnement et de la Maîtrise de l'Énergie (ADEME) and Deakin University. Contract N° TEZ13-03.

S.B., F.C., D.R., R.K., P.C.H. and M.F. also acknowledge the Australian Research Council Centre of Excellence for Electromaterials Science through grant CE140100012.

REFERENCES

(1) Armand, M.; Axmann, P.; Bresser, D.; Copley, M.; Edström, K.; Ekberg, C.; Guyomard, D.; Lestriez, B.; Novák, P.; Petranikova, M.; Porcher, W.; Trabesinger, S.; Wohlfahrt-Mehrens, M.; Zhang, H. Lithium-ion batteries – Current state of the art and anticipated developments. *J. Power Sources* **2020**, *479*, 228708.

(2) Choi, J. W.; Aurbach, D. Promise and Reality of Post-Lithium-Ion Batteries with High Energy Densities. *Nat. Rev. Mater.* **2016**, *1*, 16013.

(3) Obrovac, M. N.; Christensen, L. Structural Changes in Silicon Anodes During Lithium Insertion/Extraction. *Electrochem. Solid-State Lett.* **2004**, *7*, 93–96.

(4) Jin, Y.; Zhu, B.; Lu, Z.; Liu, N.; Zhu, J. Challenges and Recent Progress in the Development of Si Anodes for Lithium-ion Battery. *Adv. Energy Mater.* **2017**, *7*, 1–17.

(5) Wu, F.; Maier, J.; Yu, Y. Guidelines and Trends for Next-Generation Rechargeable Lithium and Lithium-Ion Batteries. *Chem. Soc. Rev.* **2020**, *49*, 1569–1614.

(6) Sanchez-Ramirez, N.; Assresahegn, B. D.; Torresi, R. M.; Bélanger, D. Producing High-Performing Silicon Anodes by Tailoring Ionic Liquids as Electrolytes. *Energy Storage Mater*. **2020**, *25*, 477–486.

(7) Mazouzi, D.; Lestriez, B.; Roué, L.; Guyomard, D. Silicon Composite Electrode with High Capacity and Long Cycle Life. *Electrochem. Solid-State Lett.* **2009**, *12*, A215–A218.

(8) Oumellal, Y.; Delpuech, N.; Mazouzi, D.; Dupré, N.; Gaubicher, J.; Moreau, P.; Soudan, P.; Lestriez, B.; Guyomard, D. The Failure Mechanism of Nano-Sized Si-Based Negative Electrodes for Lithium Ion Batteries. *J. Mater. Chem.* **2011**, *21*, 6201–6208.

(9) Nguyen, B. P. N., Chazelle, S., Cerbelaud, M., Porcher, W.; Lestriez, B. Manufacturing of Industry-Relevant Silicon Negative Composite Electrodes for Lithium Ion-Cells. *J. Power Sources* **2014**, *262*, 112–122.

(10) Mazouzi, D.; Karkar, Z.; Hernandez, C.R. ; Manero, P.J.; Guyomard, D.; Roué, L.; Lestriez, B. Critical Roles of Binders and Formulation at Multiscales of Silicon-Based Composite Electrodes. *J. Power Sources* **2015**, *280*, 533–549.

(11) Achiha, T.; Nakajima, T.; Ohzawa, Y.; Koh, M.; Yamauchi, A.; Kagawa, M.; Aoyama, H. Electrochemical Behavior of Nonflammable Organo-Fluorine Compounds for Lithium Ion Batteries. *J. Electrochem. Soc.* **2009**, *156*, A483–A488.

(12) Araño, K.; Gautier, N. ; Kerr, R. ; Lestriez, B. ; Le Bideau, J. ; Howlett, P. C. ; Guyomard, D. ; Forsyth, M.; Dupre, N.; Editors' Choice—Understanding the Superior Cycling Performance of Si Anode in Highly Concentrated Phosphonium-Based Ionic Liquid Electrolyte. *J. Electrochem. Soc.* **2020**, *167*, 120520–120530.

(13) Assresahegn, B. D.; Daniel, B. Synthesis of Binder-like Molecules Covalently Linked to Silicon Nanoparticles and Application as Anode Material for Lithium-Ion Batteries without the Use of Electrolyte Additives. *J. Power Sources* **2017**, *345*, 190–201.

(14) Patnaik, S. G.; Jayakumar, T. P.; Sawamura, Y.; Matsumi, N. Defined Poly (Borosiloxane) as an Artificial Solid Electrolyte Interphase Layer for Thin-Film Silicon Anodes. *ACS Appl. Energy Mater.* **2012**, *4*, 2241–2247.

(15) Jo, H.; Kim, J.; Nguyen, D.; Kang, K.K.; Jeon, D.; Yang, A.; Song, S. Stabilizing the Solid Electrolyte Interphase Layer and Cycling Performance of Silicon − Graphite Battery Anode by Using a Binary Additive of Fluorinated Carbonates. *J. Phys. Chem. C* **2016**, ***120***, 22466–22475.

(16) Lindgren, F.; Xu, C.; Niedzicki, L.; Marcinek, M.; Younesi, R. SEI Formation and Interfacial Stability of a Si Electrode in a LiTDI-Salt Based Electrolyte with FEC and VC Additives for Li-Ion Batteries. *ACS Appl. Mater. Interfaces* **2016**, *8*, 15758–15766.

(17) Zhu, G., Yang, S., Wang, Y., Qu, Q.; Zheng, H. Dimethylacrylamide, A Novel Electrolyte Additive, can Improve the Electrochemical Performances of Silicon Anodes in Lithium-Ion Batteries. *RSC Adv.* **2019**, *9*, 435–443.

(18) Han, B.; Liao, C.; Dogan, F.; Trask, S. E. ; Lapidus, S. H.; Vaughey, J. T.; Key, B. Using Mixed Salt Electrolytes to Stabilize Silicon Anodes for Lithium-Ion Batteries via in Situ Formation of Li-M-Si Ternaries (M = Mg, Zn, Al, Ca). *ACS Appl. Mater. Interfaces* **2019**, *11*, 29780–29790.

(19) Xu, Z.; Yang, J.; Li, H.; Nuli, Y.; Wang, J. Electrolytes for Advanced Lithium Ion Batteries Using Silicon-Based Anodes. *J. Mater. Chem. A* **2019**, *7*, 9432–9446.

(20) Girard, G. M. A.; Hilder, M.; Zhu, H.; Nucciarone, D.; Whitbread, K.; Zavorine, S.; Moser, M.; Forsyth, M.; Macfarlane, D. R.; Howlett, P. C. Electrochemical and Physicochemical Properties of Small Phosphonium Cation Ionic Liquid Electrolytes with High Lithium Salt Content. *Phys. Chem. Chem. Phys.* **2015**, *17*, 8706–8713.

(21) Salem, N.; Zavorine, S.; Nucciarone, D.; Whitbread, K.; Moser, M.; Abu-Lebdeh, Y. Physical and Electrochemical Properties of Some Phosphonium-Based Ionic Liquids and the Performance of Their Electrolytes in Lithium-Ion Batteries Physical and Electrochemical Properties of Some Phosphonium-Based Ionic Liquids and the Performance of Their. *J. Electrochem. Soc.* **2017**, *164*, H5202–H5209.

(22) Arano, K.; Begic, S.; Chen, F.; Rakov, D.; Mazouzi, D. Gautier, N. Kerr, R.; Lestriez, B.; Le Bideau, J.; Howlett, P. C.; Guyomard, D.; Forsyth, M.; Dupre, N. Tuning the Formation and Structure of the Silicon Electrode/Ionic Liquid Electrolyte Interphase in Superconcentrated Ionic Liquids. *ACS Appl. Mater. Interfaces* **2021**, ***13***, 28281–28294.

(23) Pathirana, T.; Rakov, D.A.; Chen, F.; Forsyth, M.; Kerr, R.; Howlett, P.C. Improving Cycle Life through Fast Formation Using a Superconcentrated Phosphonium Based Ionic Liquid Electrolyte for Anode-Free and Lithium Metal Batteries. *ACS Appl. Energy Mater.* **2021**, *4*, 6399–6407.

(24) Rakov, D.; Hasanpoor, M.; Baskin, A.; Lawson, J. W.; Chen, F.; Cherepanov, P. V.; Simonov, A. N.; Howlett, P.C.; Forsyth, M.; Stable and Efficient Lithium Metal Anode Cycling through Understanding the Effects of Electrolyte Composition and Electrode Preconditioning. *Chem. Mater.* **2021**, *34*, 165–177.

(25) Hwang, J.; Matsumoto, K.; Hagiwara, R. Symmetric Cell Electrochemical Impedance Spectroscopy of Na2FeP2O7 Positive Electrode Material in Ionic Liquid Electrolytes. *J. Phys. Chem. C* **2018**, *122*, 26857–26864.

(26) Liu, Q.; Jiang, W.; Munoz, M.J.P.; Liu, Y.; Yang, Z.; Bloom, I.; Dzwiniel, T.L.; Li, Y.; Pupek, K.Z.; Zhang, Z. Stabilized Electrode/Electrolyte Interphase by a Saturated Ionic Liquid Electrolyte for High-Voltage NMC532/Si-Graphite Cells. *ACS Appl. Mater. Interfaces* **2020**, *12*, 23035–23045.

(27) Nguyen, B. P. N.; Gaubicher, J.; Lestriez, B. Analogy Between Electrochemical Behaviour of Thick Silicon Granular Electrodes for Lithium Batteries and Fine Soils Micromechanics. *Electrochim. Acta* **2014**, *120*, 319–326.

(28) Karkar, Z.; Mazouzi, D.; Hernandez, C.R.; Guyomard, D.; Roué, L.; Lestriez, B. Threshold-Like Dependence of Silicon-Based Electrode Performance on Active Mass Loading and Nature of Carbon Conductive Additive. *Electrochim. Acta* **2016**, *215*, 276–288.

(29) Forsyth, M.; Girard, G. M. A.; Basile, A.; Hilder, M.; MacFarlane, D. R.; Chen, F.; Howlett, P. C. Inorganic-Organic Ionic Liquid Electrolytes Enabling High Energy-Density Metal Electrodes for Energy Storage. *Electrochim. Acta* **2016**, *220*, 609–617.

(30) Girard, G. M. A.; Hilder, M.; Dupre, N.; Guyomard, D.; Nucciarone, D.; Whitbread, K.; Zavorine, S.; Moser, M.; Forsyth, M.; MacFarlane, D. R.; Howlett, P. C. Spectroscopic Characterization of the SEI Layer Formed on Lithium Metal Electrodes in Phosphonium Bis(fluorosulfonyl)imide Ionic Liquid Electrolytes. *ACS Appl. Mater. Interfaces* **2018**, *10*, 6719–6729.

(31) Low, J.; Kreider, M. L.: Pulsifer, D. P.; Jones, A. S.; Gilani, T. H. Band Gap Energy in Silicon. *Am. J. Undergrad. Res.* **2008**, *7*, 27–32.

(32) O'Reilly, E. P. The Electronic Structure of Amorphous Carbon. *J. Non. Cryst. Solids* **1987**, *98*, 1095–1102.

(33) Klein, J. M.; Panichi, E.; Gurkan, B. Potential Dependent Capacitance of [EMIM][TFSI], [N1114][TFSI] and [PYR13][TFSI] Ionic Liquids on Glassy Carbon. *Phys. Chem. Chem. Phys.* **2019**, *21*, 3712–3720.

(34) Massiot, D. dmfit. *https://nmr.cemhti.cnrs-orleans.fr/dmfit/* as accessed in December 2021.

(35) Massiot, D.; Fayon, F.; Capron, M.; King, I.; Le Calvé, S.; Alonso, B.; Durand, J.O.; Bujoli, B.; Gan, Z.; Hoatson, G. Modelling One- and Two-Dimensional Solid-State NMR Spectra. *Magn. Reson. Chem.* **2002**, *40*, 70–76.

(36) Dupré, N.; Moreau, P.; De Vito, E.; Quazuguel, L.; Boniface, M.; Bordes, A.; Rudisch, C.; Bayle-Guillemaud, P.; Guyomard, D. Multiprobe Study of the Solid Electrolyte Interphase on Silicon-Based Electrodes in Full-Cell Configuration. *Chem. Mater.* **2016**, *28*, 2557–2572.

(37) Cuisinier, M.; Martin, J. F.; Moreau, P.; Epicier, T.; Kanno, R.; Guyomard, D.; Dupré, N. Quantitative MAS NMR Characterization of the LiMn1/2Ni1/2O2 Electrode/Electrolyte Interphase. *Solid State Nucl. Magn. Reson.* **2012**, *42*, 51–61.

(38) Hilder, M.; Howlett, P.C.; Saurel, D.; Anne, H.; Casas, M.; Armand, M.; Macfarlane, D.R.; Forsyth, M. Stable cycling of NaFePO4 cathodes in high salt concentration ionic liquid electrolytes **2018**, *406*, 70–80.

(39) Kerr, R.; Singh, N.; Arthur, T. S.; Pathirana, T.; Mizuno, F.; Takechi, K.; Forsyth, M.; Howlett, P.C. Water-tolerant lithium metal cycling in high lithium concentration phosphonium-based ionic liquid electrolytes. *Sustain. Energy Fuels* **2018**, *2*, 2276–2283.

(40) Eom, K.; Joshi, T.; Bordes, A.; Do, I.; Fuller, T. F. The design of a Li-ion full cell battery using a nano silicon and nano multi-layer graphene composite anode. *J. Power Sources* **2014**, *249*, 118–124.

(41) Kerr, R.; Mazouzi, D.; Eftekharnia, M.; Lestriez, B.; Dupré, N.; Forsyth, M.; Guyomard, D.; Howlett, P.C. High-Capacity Retention of Si Anodes Using a Mixed Lithium/Phosphonium Bis(fluorosulfonyl)imide Ionic Liquid Electrolyte. *ACS Energy Lett.* **2017**, *2*, 1804–1809.

(42) Beattie, S. D.; Loveridge, M. J.; Lain, M. J.; Ferrari, S.; Polzin, B. J.; Bhagat, R.; Dashwood, R. Understanding capacity fade in silicon based electrodes for lithium- ion batteries using three electrode cells and upper cut-off voltage studies. *J. Power Sources* **2016**, *302*, 426–430.

(43) Dose, W. M.; Maroni, V. A.; Piernas-Muñoz, M. J.; Trask, S. E.; Bloom, I.; Johnson, C. S.; Assessment of Li-Inventory in Cycled Si-Graphite Anodes Using LiFePO 4 as a Diagnostic Cathode . *J. Electrochem. Soc.* **2018**, *165*, A2389–A2396.

(44) Ruther, R. E.; Hays, K.A.; An, S. J.; Li, J.; Wood, D. L.; Nanda, J. Chemical Evolution in Silicon-Graphite Composite Anodes Investigated by Vibrational Spectroscopy. *ACS Appl. Mater. Interfaces* **2018**, *10*, 18641–18649.

(45) Wagner, N. P.; Asheim, K.; Vullum-Bruer, F.; Svensson, A. M. Performance and failure analysis of full cell lithium ion battery with LiNi0.8Co0.15Al0.05O2 and silicon electrodes. *J. Power Sources* **2019**, *437*, 226884.

(46) Gilbert, J. A.; Shkrob, I. A.; Abraham, D. P. Transition Metal Dissolution, Ion Migration, Electrocatalytic Reduction and Capacity Loss in Lithium-Ion Full Cells. *J. Electrochem. Soc.* **2017**, *164*, A389–A399.

(47) Michalak, B.; Berkes, B. B.; Sommer, H.; Brezesinski, T.; Janek, J. Electrochemical cross-talk leading to gas evolution and capacity fade in LiNi0.5Mn1.5O4/graphite full-cells. *J. Phys. Chem. C* **2017**, *121*, 211–216.

(48) Knehr, K. W.; Hodson, T.; Bommier, C.; Davies, G.; Kim, A.; Steingart, D. A. Understanding Full-Cell Evolution and Non-chemical Electrode Crosstalk of Li-Ion Batteries. *Joule* **2018**, *2*, 1146–1159.

(49) Tornheim, A.; Sahore, R.; He, M.; Croy, J. R.; Zhang, Z. Preformed Anodes for High-Voltage Lithium-Ion Battery Performance: Fluorinated Electrolytes, Crosstalk, and the Origins of Impedance Rise. *J. Electrochem. Soc.* **2018**, *165*, A3360–A3368.

(50) Betz, J.; Brinkmann, J. P.; Nölle, R.; Lürenbaum, C.; Kolek, M.; Stan, M. C.; Winter, M.; Placke, T. Cross Talk between Transition Metal Cathode and Li Metal Anode: Unraveling Its Influence on the Deposition/Dissolution Behavior and Morphology of Lithium. *Adv. Energy Mater.* **2019**, *9*, 1–10.

(51) Guo, Y. G. Minimized lithium trapping for high initial coulombic efficiency of silicon anodes. *Wuli Huaxue Xuebao/ Acta Phys. - Chim. Sin.* **2020**, *36*, 1–9.

(52) Usubelli, C.; Besli, M.M.; Kuppan, S.; Jiang, N.; Metzger, M.; Dinia, A.; Christensen, J.; Gorlin, Y. Understanding the Overlithiation Properties of LiNi0.6Mn0.2Co0.2O2 Using Electrochemistry and Depth-Resolved X-ray Absorption Spectroscopy. *J. Electrochem. Soc.* **2020**, *167*, 080514.

(53) Islam, M. M.; Alam, M. T.; Ohsaka, T. Electrical Double-layer Structure in Ionic Liquids: A Corroboration of the Theoretical Model by Experimental Results. *J. Phys. Chem. C* **2008**, *112*, 16568–16574.

(54) Haskins, J. B.; Wu, J. J.; Lawson, J. W. Computational and Experimental Study of Li-Doped Ionic Liquids at Electrified Interfaces. *J. Phys. Chem. C* **2016**, *120*, 11993–12011.

(55) Lockett, V.; Sedev, R.; Ralston, J.; Horne, M.; Rodopoulos, T. Differential Capacitance of the Electrical Double Layer in Imidazolium-Based Ionic Liquids: Influence of Potential, Cation Size, and Temperature. *J. Phys. Chem. C* **2008**, *112*, 7486–7495.

(56) Tułodziecki, M.; Tarascon, J. M.; Taberna, P. L.; Guéry, C. Catalytic reduction of TFSI-containing ionic liquid in the presence of lithium cations. *Electrochem. commun.* **2017**, *77*, 128–132.

(57) Xiong, J.; Dupré, N.; Moreau, P.; Lestriez, B. From the Direct Observation of a PAA-Based Binder Using STEM-VEELS to the Ageing Mechanism of Silicon / Graphite Anode with High Areal Capacity Cycled in an FEC-Rich and EC-Free Electrolyte *Adv. Energy Mater.* **2022**, *12*, 2103348.

(58) Sharova, V.; Moretti, A.; Diemant, T.; Varzi, A.; Behm, R.J.; Passerini, S. Comparative study of imide-based Li salts as electrolyte additives for Li-ion batteries. *J. Power Sources* **2018**, *375*, 43–52.

(59) Zhang, X. Q.; Chen, X.; Hou, L. P.; Li, B. Q.; Cheng, X. B.; Huang, J. Q.; Zhang, Q. Regulating Anions in the Solvation Sheath of Lithium Ions for Stable Lithium Metal Batteries. *ACS Energy Lett.* **2019**, *4*, 411–416.

(60) Fan, X.; Chen, L.; Ji, X.; Deng, T.; Hou, S.; Chen, J.; Zheng, J.; Wang, F.; Jiang, J.; Xu, K.; Wang, C. Highly Fluorinated Interphases Enable High-Voltage Li-Metal Batteries. *Chem.* **2018**, *4*, 174–185.

(61) Philippe, B.; Dedryvere, R.; Gorgoi, M.; Rensmo, H.; Gonbeau, D.; Edström, K. Improved performances of nanosilicon electrodes using the salt LiFSI: A photoelectron spectroscopy study. *J. Am. Chem. Soc.* **2013**, *135*, 9829–9842.

(62) Hasanpoor, M.; Saurel, D.; Barreno, R. C.; Fraysse, K.; Echeverría, M.; Jáuregui, M.; Bonilla, F.; Greene, G. W.; Kerr, R.; Forsyth, M.; Howlett, P. C. Morphological Evolution and Solid-Electrolyte Interphase Formation on LiNi0.6Mn0.2Co0.2O2 Cathodes Using Highly Concentrated Ionic Liquid Electrolytes. *ACS Appl. Mater. Interfaces* **2022**, *14*, 13196–13205.

(63) Meyer, B. M.; Leifer, N.;;; Sakamoto, S.; Greenbaum, S. G.; Grey, C. P. High Field Nultinuclear NMR Investigation of the SEI Layer in Lithium Rechargeable Batteries. *Electrochem. Solid-State Lett.* **2005**, ***8***, 5–9.

(64) Mousavi, A.; Bensalem, A.; Gee, B. Low-Temperature Synthesis of a Green Material for Lithium-Ion Batteries Cathode. *Green Chem. Lett. Rev.* **2010**, *3*, 135–142.

(65) Delpuech, N.; Dupré, N.; Mazouzi, D.; Gaubicher, J.; Moreau, P.; Bridel, J.S.; Guyomard, D.; Lestriez, B. Correlation Between Irreversible Capacity and Electrolyte Solvents Degradation Probed by NMR in Si-Based Negative Electrode of Li-Ion Cell. *Electrochem. commun.* **2013**, *33*, 72–75.

(66) See, K. A.; Leskes, M.; Griffin, J. M.; Britto, S.; Matthews, P. D.; Emly, A.; Van Der Ven, A.; Wright, D.S.;. Morris, A.J; Grey, C.P.; Seshadri, R. Ab Initio Structure Search

and In Situ 7Li NMR Studies of Discharge Products in the Li-S Battery System. *J. Am. Chem. Soc.* **2014**, *136*, 16368–16377.

(67) Cao, C.; Abate, I. I.; Sivonxay, E.;Shyam, B.; Jia, C. J.; Moritz, B.; Devereaux, T.; Persson, K. A. ; Steinruck, H. G.; Toney, M. F. Solid Electrolyte Interphase on Native Oxide-Terminated Silicon Anodes for Li-Ion Batteries. *Joule* **2019**, *3*, 762–781.

(68) Michan, A. L.; Divitini, G.; Pell, A. J.; Leskes, M.; Ducati, C.; Grey, C.P. Solid Electrolyte Interphase Growth and Capacity Loss in Silicon Electrodes. *J. Am. Chem. Soc.* **2016**, *138*, 7918–7931.

(69) Jiao, S.; Zheng, J.; Li, Q.; Li, X.; Engelhard, M.H.; Cao, R.; Zhang, J.G.; Xu, W. Behavior of Lithium Metal Anodes under Various Capacity Utilization and High Current Density in Lithium Metal Batteries. *Joule* **2018**, *2*, 110–124.

(70) Horstmann, B.; Shi, J.; Amine, R.; Werres, M.; He, X.; Jia, H.; Hausen, F.; Cekic-Laskovic, I.; Wiemers-Meyer, S.; Lopez, J.; Galvez-Aranda, D.; Baakes, F.; Bresser, D.; Su, C.C.; Xu, Y.; Xu, W.; Jakes, P.; Eichel, R.A.; Figgemeier, E.; Krewer, U.; Seminario, P.B.; Balbuena, J.M.; Wang, C.; Passerini, S.; Shao-Horn, Y.; Winter, M.; Amine, K.; Kostecki, R.; Latz,Strategies A. Towards Enabling Lithium Metal in Batteries: Interphases and Electrodes. *Energy Environ. Sci.* **2021**, *14*, 5289–5314.

TOC graphics

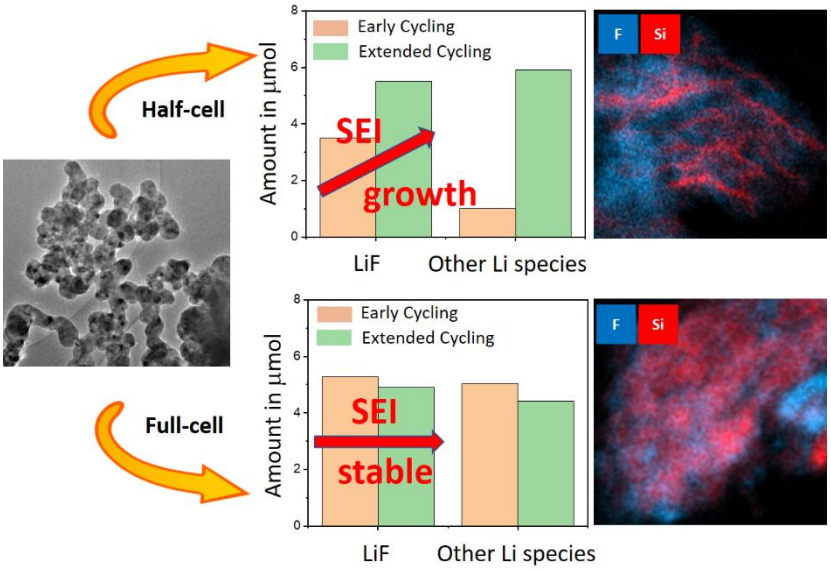
Half-cell
Full-cell
Amount in µmol
Early Cycling
Extended Cycling
SEI
growth
LiF
Other Li species
F
Si
SEI
stable